February 18, 2013

Combined Topographic, Spectroscopic, and Model Analyses of Inhomogeneous Energetic Coupling of Linear Light Harvesting Complex Ii Aggregates in Native Photosynthetic Membranes

Suneth P. Rajapaksha
Yufan He
Hong Peter Lu, *Bowling Green State University*

PCCP

RSC Publishing

PAPER

Combined topographic, spectroscopic, and model analyses of inhomogeneous energetic coupling of linear light harvesting complex II aggregates in native photosynthetic membranes†

Cite this: *Phys. Chem. Chem. Phys.*, 2013, **15**, 5636

Suneth P. Rajapaksha, Yufan He and H. Peter Lu*

Light harvesting by LH1 and LH2 antenna proteins in the photosynthetic membranes of purple bacteria has been extensively studied in recent years for the fundamental understanding of the energy transfer dynamics and mechanism. Here we report the inhomogeneous structural organization of the LH2 complexes in photosynthetic membranes, giving evidence for the existence of energetically coupled linear LH2 aggregates in the native photosynthetic membranes of purple bacteria. Focusing on systematic model analyses, we combined AFM imaging and spectroscopic analysis with energetic coupling model analysis to characterize the inhomogeneous linear aggregation of LH2. Our AFM imaging results reveal that the LH2 complexes form linear aggregates with the monomer number varying from one to eight and each monomer tilted along the aggregated structure in photosynthetic membranes. The spectroscopic results support the attribution of aggregated LH2 complexes in the photosynthetic membranes, and the model calculation values for the absorption, emission and lifetime are consistent with the experimentally determined spectroscopic values, further proving a molecular-level understanding of the energetic coupling and energy transfer among the LH2 complexes in the photosynthetic membranes.

Received 10th October 2012,
Accepted 18th February 2013

DOI: 10.1039/c3cp43582b

www.rsc.org/pccp

Introduction

The conversion of light energy to chemical energy in photosynthetic bacteria starts at the membrane protein complexes, light harvesting complexes and reaction centers, activating the entire photosynthesis pathway.[1–4] The photosynthetic membrane of purple bacteria contains two types of protein complexes involving in light harvesting: the Light Harvesting Complex I (LH1) and the Light Harvesting Complex II (LH2).[5,6] LH2 complexes are present in variable amounts, absorbing light energy. The energy received by LH1 complexes from the LH2 complexes is ultimately transferred to the reaction centers[3,7–9] to initiate the charge separation and charge transport across the membrane, which complete the initial photosynthesis process.[5,6]

In LH1, 32 bacteriochlorophyll (BChl) units are arranged in a ring or a fragment of a ring structure surrounding the reaction center, and are responsible for the absorption at 875 nm wavelength.[10] LH2 complexes of most species including *Rhodopseudomonas acidophila* contain a symmetric ring of nine subunits[4,6,11,12] and each subunit consists of two transmembrane helix proteins (α-polypeptide in the inside and β-polypeptide in the outside of the ring), one carotenoid and three BChls (Fig. 1A).[12] The BChls are arranged to form a tightly packed ring and a loosely packed ring (Fig. 1B). The tightly packed ring of the LH2 complexes contains 18 vertically oriented BChls with <1 nm center-to-center distance between adjacent pigments and is responsible for intense absorption at around 850 nm.[10,12] The loosely packed ring has 9 BChl pigments which are oriented parallel to the plane of the membrane and absorbed at 800 nm wavelength.[6,12] The intra-protein arrangement of the BChls of LH2 and LH1,[6,13–16] as well as the ultrafast energy transfer among intra-BChls and inter-BChls[17,18] have been extensively studied; in contrast, however, the structural arrangement of LH2 complexes in the native photosynthetic membranes and energetic coupling between LH2 complexes are yet to be fully analyzed and understood. The aggregation of light capturing antenna protein complexes in the photosynthetic membrane helps in transfer of the excitation energy to the reaction center.[19–21] The stripe and circular arrangements of LH2 around LH1 have been

Department of Chemistry and Center for Photochemical Sciences, Bowling Green State University, Bowling Green, OH 43403, USA. E-mail: hplu@bgsu.edu; Fax: +1 419-372-1840

† Electronic supplementary information (ESI) available: Experimental details, sample preparations, and additional AFM images showing linear aggregates of LH2 proteins in the photosynthetic membranes of different bacterial species. See DOI: 10.1039/c3cp43582b

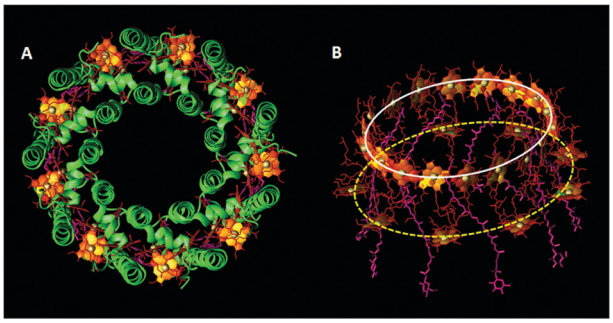

Fig. 1 The structure of the *Rhodopseudomonas acidophila* LH2 complex (Protein Data Bank ID 2FKW). (A) The top view of the LH2 complex. The polypeptides are shown in green. The BChls are shown in red line style with porphyrins in orange color plates. Carotenoids are shown in purple. (B) The pigment arrangement in the LH2 complex (protein parts are not shown for clarity). The white color solid line circle represents the B850 pigment ring and the yellow color dashed line circle represents the B800 ring. Carotenoids are shown in purple. The molecular graphics are developed with Visual Molecular Dynamics (VMD).[34]

proposed to describe the structural arrangement of LH2 complexes and LH2–LH1 coupling in the photosynthetic membranes.[1,22–25] In recent years, the nanometric spatial arrangement of LH2 complexes in the photosynthetic membranes has been studied extensively by Atomic Force Microscopy (AFM).[5,26–31] We have previously reported: (1) AFM imaging observations of linear aggregation of the LH2 complexes in the native photosynthetic membranes, (2) spectral red shift in absorption and emission of LH2 complexes in photosynthetic membranes,[32] and (3) spectral fluctuations associated with energy transfer among the LH2 complexes in the photosynthetic membranes.[33] Nevertheless, the aggregation of LH2 complexes has not been systematically analyzed in order to reveal the nature of the LH2 energetic interactions prior to this current work.

LH2 antenna proteins are responsible for absorbing light energy for photosynthesis, and efficient intra- and inter-molecular energy transfers of LH2 complexes are important for the overall efficiency of the light harvesting mechanism. Extensive advancements have been made in analysis of the intramolecular energy transfer ultrafast dynamics in LH1 and LH2 in recent years; whereas, there is still lack of experimental analysis of intermolecular energy transfer dynamics, especially among the LH2 molecules in the photosynthetic membranes. The difficulties are due to the complexities in the relation of the energy transfer dynamics with the local environments in the membranes. Therefore, combined topographic measurements and spectroscopic analyses are helpful to dissect the structure regulated inter-LH2 energy transfer processes in light harvesting photosynthesis membranes. In this article, we report the existence of energetically coupled, linearly aggregated LH2 complexes by correlating the AFM topographic imaging and spectroscopic measurements with aggregate energetic coupling theoretical model calculation to characterize the nature of LH2 aggregation in the native photosynthetic membranes.

Experimental section

The details of the bacterial growth, the sample preparation for the AFM imaging and the spectroscopic measurements were reported earlier[32,33] and are also listed in the ESI† (Fig. S1 and S2). Briefly, AFM images were recorded in the tapping mode under ambient conditions. A closed-loop multipurpose AFM scanner (Agilent 5500 SPM Microscope, Agilent technologies) and an ultra-sharp AFM tip (Mikromasch) with 0.6 N m^{-1} spring constant and ~75 kHz resonant frequency were used in the measurements with the line scanning frequency of 1–2 Hz for a 512 × 512 pixels^2 image.

In spectroscopic measurements, the samples were excited using a 795 nm pulse laser (100 fs pulses at a repetition rate of 76 MHz, Ti:sapphire laser system, Mira 900, Coherent) with an average incident power of 3–4 μW. The images of single membrane fragments of LH2 were recorded using an inverted confocal microscope (Axiovert-200, Zeiss). A dichroic mirror (815 dclp, Chroma Technology) was used to direct the laser beam to the sample *via* a high numerical aperture objective (1.3 NA, 63×, oil immersion, Zeiss). The sample was spin-coated, and raster scanned with respect to the laser focus by using an *x*–*y* electropiezo closed-loop scanning stage (H100, Mad City Lab). The emitted fluorescence was collected by the same objective before filtering from a long pass filter (HQ825LP, Chroma Technology). For both imaging and lifetime measurements, two Si avalanche photodiode single photon counting modules (APDs) were used as detectors (SPCM-AQR-14, PerkinElmer, for imaging and SPDM, Micro Photon Devices, for lifetime measurements). The fluorescence images (100 × 100 pixels^2) were acquired by continuous raster scanning of the sample at a rate of 4 ms per pixel.

The ensemble-averaged absorption spectra were recorded using a VARIAN Cary 50 Scan UV-Visible Spectrophotometer and the emission spectra were recorded using a Quantamaster NIR Fluorometer (Photon Technology International).

The membrane fragments from several photosynthetic bacterial species, *Rhodobacter sphaeroides* (strain 2.4.1 and strain ATCC17025) and *Rhodospirillum fulvum*, were studied and the linearly aggregated LH2 complexes in the membrane were observed in both species (ESI,† Fig. S2–S4). The membrane fragments of the photosynthetic organelles tend to form folded particles with curved structures in solutions or on untreated glass surfaces.[2] In our experiments, the fragments are spread out on a mica surface to have a single layer of membrane LH2 complexes for AFM imaging analysis. To ensure the spreading of a monolayer on the substrate surface, the membrane fragments in solution are spread on a freshly cleaved $MgCl_2$ treated mica surface and rinsed with buffer to remove possible multilayers of membrane patches (the detailed description of sample preparation is given in ESI†). Although all the examined bacterial species show the existence of the linear LH2 aggregates in the photosynthetic membranes, we focus our study on the membrane fragments from the wild-type *Rhodobacter sphaeroides* (strain 2.4.1).

Energetic coupling in LH2 aggregates

The AFM and spectroscopic observations of LH2 in the bacterial photosynthetic membrane allow us to develop an energetic coupling model by combining experimental characterization and a simple dipole–dipole coupling theory related with *J* type aggregates.

The specific experimental results involving the data analytical model are (1) the small tilting angle of the aggregated LH2 complexes in the biological membrane measured by our AFM imaging analysis; (2) the spectral red shifts in the absorption and emission of the membrane LH2 complexes; and (3) the distribution of the LH2 protein numbers involving in the linear aggregates.

The transition dipole interactions of the energetically coupled aggregates lead to the excited state energy splitting that is associated with the energy gap between the ground and excited states, eventually deciding the direction of the spectral shift, *i.e.*, red or blue shifts.[35] Depending on the spectral shifting direction, the molecular aggregates can be categorized into two types: *J* aggregates with a red spectral shift and *H* aggregates with a blue spectral shift.[35–39] Using the point dipole approximation, *J* and *H* type aggregates are defined by the angle between the direction of the transition dipole moment and the plane of the molecular aggregate.[35] When the angle is less than 54.8°, the excitonic coupling becomes negative and the aggregate behaves as a *J* type aggregate showing a red spectral shift for absorption and emission (Fig. 2A1), and when the angle is higher than 54.8°, the aggregate shows a blue spectral shift for both absorption and emission behaving as a *H* type aggregate (Fig. 2A2). These two aggregate types have been extensively studied over the last several decades using various technical approaches to characterize the nature of aggregates.[40–45]

Generally, the inter-LH2 van der Waals interactions of linear LH2 aggregates are concentrated at the junctions between LH2 complexes making the electronic overlap small (Fig. 2B1) so that the individual characteristics of each LH2 complex are preserved. Hence, electronically interacting LH2 complexes can be treated by neglecting the interactions at interfaces and focusing only on the interactions of transition dipole–dipole between the LH2 complexes that are responsible for coherent delocalization of excitons over the aggregate. There is a major difference between the intra-LH2 chromophore dipole–dipole coupling (Fig. 2B2) and the inter-LH2 (between the overall dipoles of adjacent LH2 proteins) dipole–dipole coupling. The intra-LH2 transition dipole–transition dipole coupling is strong and has been widely studied; whereas, the inter-LH2 transition dipole–dipole coupling is significantly weaker and can be better studied using our topographic, spectroscopic, and theoretical modeling study approach (ESI,† S5 and Fig. S1). Furthermore, the tilted card pack configuration of the LH2 complexes in our model structural configuration (Fig. 2B3) ensures both the required angle for resonant dipole–dipole interactions and the distance between two molecules for necessary strength of the interactions.[46] Dipole interactions have been reported as the major type of interaction in deciding the coupling strength and the energy of the excitation band of the *J* aggregated structures.[47] Although the transition dipole–dipole interactions of molecules in the *J* aggregates delocalize the excitons over the aggregate, using the typical Förster theory to explain the rate of energy transfer is not necessarily sufficient, and an alternative or a modified Förster mechanism for the energy transfer process has been reported extensively.[48–51]

To understand the energy transfer coupling among the LH2 proteins in the photosynthetic membrane, we develop an aggregate energetic coupling model based on experimentally measured structural configuration associated with the energetic coupling between LH2 molecules for delocalization of excitons and long range energy transfer. Fig. 2B3 shows the tilted card pack model of two LH2 complexes in a linear array and parameters used for aggregate energetic coupling and spectroscopic calculation. The tilting angle (θ) is the angle between the direction of the transition dipole moment (the combined transition dipole moment of all the BChls in a LH2 complex) and the plane of the LH2 aggregate. Sauer *et al.* comprehensively explained the details of the transition dipole moments of nanomeric LH2 structures.[52] Briefly, the arrangement of the 9 subunits in a LH2 complex brings the symmetry of the system to C9 (Fig. 2B). Although the LH2 molecules have 27 excitonic states generated from 27 BChls, the C9 symmetry of the LH2 complexes has significantly reduced the complexity of the absorption spectrum. Out of the 27 transitions, 3 are non-degenerate in energy and the other 24 form 12 degenerate pairs. However, only three of the degenerate pairs show non-zero dipole strengths. The intensity of the absorption is shared among three transitions (one non-degenerate and two degenerate). The degenerate transition moment vectors (25.43 Debye (D) and 18.80 D) are in the plane perpendicular to the C9 axis and the non-degenerate transition with 3.250 D magnitude positions along the C9 axis. It has been identified that the dominant transition dipole moments in the spectral region are aligned perpendicular to the common axis.[52] Therefore, the highest transition dipole moment (25.43 D) was assigned to the

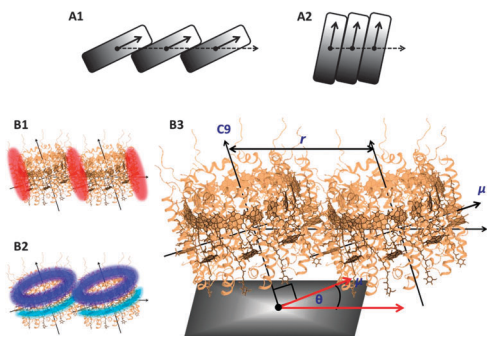

Fig. 2 Conceptual sketches of the energetic couplings. (A) Two types of molecular aggregations. The plane of the molecular aggregate is shown with a dashed arrow and the directions of the transition dipole moment are shown with solid arrows. (A1) Molecular arrangement of *J* aggregates and (A2) Molecular arrangement of *H* aggregates. (B) The interactions of intra and inter LH2 complexes and the model of the aggregated LH2 complexes in the photosynthetic membrane. (B1) The interactions at the junctions of neighboring LH2 complexes (red). (B2) The intra-LH2 interactions (B850 ring (blue) and B800 ring (cyan)). (B3) The model for the arrangement of LH2 complexes in a linear aggregate. The interaction reported in this work is transition dipole–transition dipole (μ) interaction. The adjacent LH2 complexes in an aggregate are tightly packed and the distance between the centers of the LH2 complexes (r) is determined to be 7 nm. The tilted angle (θ) of the LH2 complexes from the plane of the membrane is $4 \pm 2°$ according our AFM topographic imaging results. The transition dipole moment (μ) with highest magnitude is tilted by θ angle to the plane of the membrane (the position of the μ in the figure is used only for the illustration purposes).

absorption peak with the highest intensity at 848 nm. Our AFM imaging analysis reveals the tight packing of the LH2 complexes in an aggregate, and specifies the distance between the centers of two neighboring LH2 complexes to be 7 nm and the tilted angle (θ) of the transition dipole (μ) along with the LH2 complexes from the plane of the membrane to be $4 \pm 2^{\circ}$, showing an agreement with the reported values.[31,53]

Most of the following calculations are essentially based on the typical aggregate energetic coupling theory.[35] The coupling constant (J) of two molecules (i and j) can be determined by using the point dipole approximation when the distance between i and j is sufficiently high.

$$J_{ij} = \frac{\mu_i \mu_j}{4\pi\varepsilon_0 \varepsilon r^3}(1 - 3\cos^2\theta) \quad (1)$$

Where μ_i and μ_j are the transition dipole moments of i and j molecules in coulomb meters (Cm). ε_0 is the permittivity of free space (8.854×10^{-12} C^2 N^{-1} m^{-2}). ε is the dielectric constant of the medium and is considered to be 2.5 for the surrounding lipid medium of the LH2 complexes.[54,55] r is the distance between the centers i and j in meters. θ is the angle between the transition dipole moment and the plane of the aggregated structure in degrees.[35] Since the μ_i, μ_j and θ values for identical monomers are constants with the length of an aggregate that are in an identical environment, the amplitude of the coupling constant is determined by the center-to-center distance (r) between i and j.

The maximum wavelength of the absorption of purified LH2 complexes is 848 nm and the excitation energy can be calculated by using the Planck–Einstein relationship.

$$\Delta E^{ex} = \frac{hc}{\lambda} \quad (2)$$

ΔE^{ex} is the excitation energy in Joules (J), h is the Planck constant (6.626×10^{-34} Js), c is the speed of light in m s^{-1} and λ is the absorption wavelength in meters. The excitation energy of an aggregate can be obtained by the following relationship between the excitation energy of the monomers and the coupling constants of an aggregate.

$$\Delta E^{ex}_{agg} = \sqrt{\Delta E^{ex^2} + 4\Delta E^{ex}\sum_{j\neq i} J_{ij}} \approx \Delta E^{ex} + 2\sum_{j\neq i} J_{ij} \quad (3)$$

ΔE^{ex}_{agg} is the excitation energy of an aggregate.

The emitted power, $\left(\overline{dE/dt}\right)_{fl}$, of a molecule is given from the equation below.

$$\overline{\left(\frac{dE}{dt}\right)}_{fl} = \left(\frac{1}{\tau}\right)\Delta E^{em} = \left(\frac{2}{3}\frac{q^2}{m}\frac{4\pi^2\nu_0^2\hat{n}}{4\pi\varepsilon_0 c^3}\right)\Delta E^{em} \quad (4)$$

Where τ is the fluorescence lifetime in seconds (s) and ΔE^{em} is the emitting energy in Joules (J). The emission wavelength of the purified LH2 complexes is 866 nm and the emitting energy can be calculated using eqn (2), q is the charge, m is the mass, ν_0 is the frequency, $\hat{n}$ is the refractive index of the medium (1.46 for lipid medium[56,57]). (q^2/m) and ν_0 can be set to $\frac{q^2}{m} = \frac{2\Delta E^{ex}}{\hbar^2}\mu^2$ and $\nu_0 = \frac{\Delta E^{ex}}{h}$, where ΔE^{ex} is the excitation energy, μ is the transition dipole moment for excitation, and $\hbar = h/2\pi$. If each oscillator (each LH2 complex) in the aggregate has the same oscillating amplitude, then the system of oscillators, N, can be considered as a single oscillator with mass Nm and charge Nq with oscillating frequency of ν_{agg}. By considering the entire aggregate as a point dipole, eqn (4) can be rewritten as:

$$\overline{\left(\frac{dE}{dt}\right)}^{agg}_{fl} = \left(\frac{1}{\tau_{agg}}\right)\Delta E^{em}_{agg} = \left(\frac{2}{3}\frac{(Nq)^2}{Nm}\frac{4\pi^2\nu_{agg}{}^2\hat{n}}{4\pi\varepsilon_0 c^3}\right)\Delta E^{em}_{agg} \quad (5)$$

The emission is always sensitive to the fluorescence quantum yield, ϕ, and if $\nu_{agg} \cong \nu_0$, the lifetime of the aggregate, τ_{agg} is;

$$\tau_{agg} = \phi\frac{1}{N}\tau \quad (6)$$

The experimentally measured fluorescence quantum yield of LH2 is 0.14.[58,59]

To calculate the emission wavelengths of aggregated LH2 complexes in the photosynthesis membrane, the transition dipole moment for emission needs to be determined. The total time-averaged radiated power, P, of an oscillating dipole[60,61] is given by,

$$P = \frac{\omega^4 \mu_{em}{}^2}{12\pi\varepsilon_0 c^3} \quad (7)$$

where μ_{em} is the transition dipole moment of the emission, ω is the angular frequency and can be replaced by $2\pi\nu$ where ν is the normal frequency. Then eqn (7) becomes,

$$P = \frac{16\pi^4\nu^4\mu_{em}{}^2}{12\pi\varepsilon_0 c^3} \quad (8)$$

Eqn (4) can be rewritten by using the relationships in eqn (2) (with the emission terms) and eqn (6) as follow:

$$\overline{\left(\frac{dE}{dt}\right)}_{fl} = \frac{\phi h\nu}{N\tau_{agg}}. \quad (9)$$

The combination of eqn (8) and eqn (9) (both equations calculate the emitted power of an oscillating dipole) gives a relationship for the transition dipole moment of the emission.

$$\mu_{em}{}^2 = \frac{3\varepsilon_0 c^3 \phi h}{4\pi^3\nu^3\tau_{agg}N} \quad (10)$$

The emission wavelength of the aggregated LH2 was calculated using eqn (3) and eqn (2) after calculating the coupling constant for the emission using eqn (1).

Results and discussion

In this work, we conduct AFM imaging and spectroscopic analysis with aggregate energetic coupling theoretical calculations to confirm the existence and characterize the spatial arrangement of the LH2 linear aggregates in the photosynthesis membrane. The linear aggregation of LH2 complexes in photosynthetic membranes was previously reported by Lu and co-workers.[32] Fig. 3A shows an AFM tapping-mode image of the photosynthetic membrane of *Rhodobacter sphaeroides* (strain 2.4.1) and the tightly packed ring-shaped structures, which have been previously

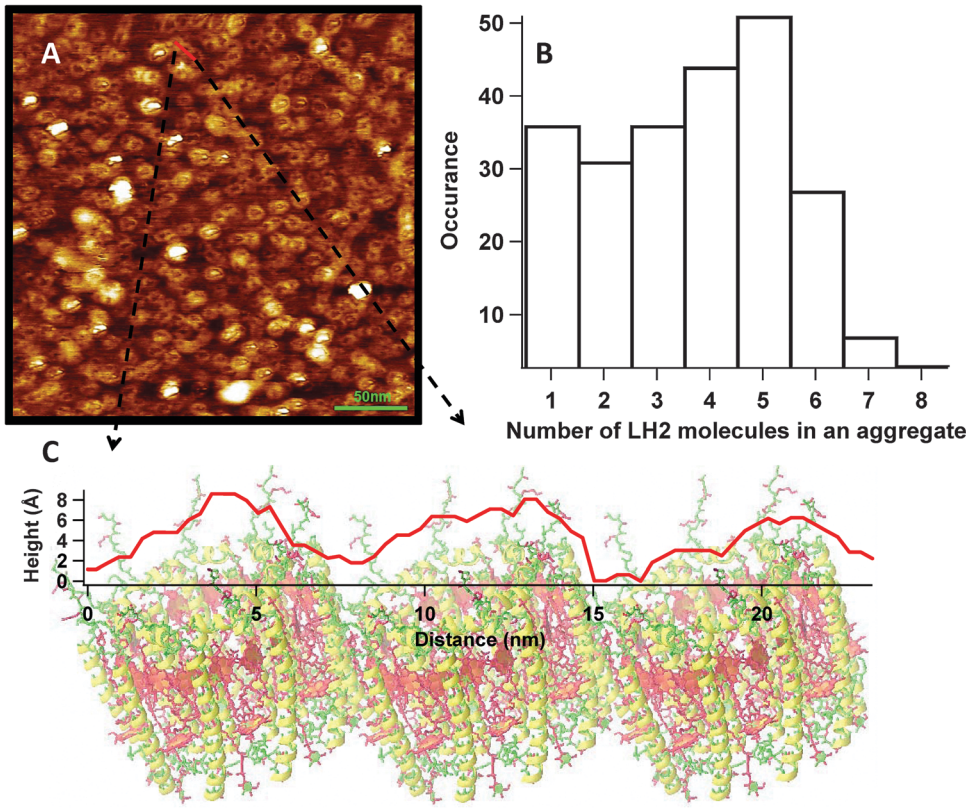

Fig. 3 Atomic Force Microscopic (AFM) analysis of the fragments of the membrane obtained from *Rhodobacter sphaeroides* (strain 2.4.1). (A) An AFM tapping mode image of the photosynthetic membrane. The circular structures are identified as the LH2 complexes and the linear aggregation is clearly observable. (B) Population distribution of LH2 aggregates in the photosynthetic membrane. The distribution is obtained from counting the numbers of the LH2 involved in each aggregate from the AFM image in A. (C) Height amplitude variation of the monotonically tilted LH2 complexes in an aggregate.

identified[32] and are further verified in this work as linearly aggregated LH2 complexes. The linear aggregates are formed with a variable number of LH2 complexes ranging from one to eight. The population densities of the aggregated LH2 complexes with different lengths are determined by counting each aggregated LH2 complex in the recorded AFM images of the native photosynthetic membrane (Fig. 3B). The population distribution of the aggregates in the membrane reveals that the aggregates with five LH2 complexes have the highest occurrence in the photosynthetic membrane. The monomer (non-aggregated LH2) to the hexamer aggregates are the most common types while the heptamer and the octamer also exist in low population densities. By examining the height topographic profile along an aggregate, we observe that the LH2 complexes in an aggregate are monotonically tilted by an angle of $4 \pm 2^{\circ}$ (Fig. 3C) to the plane of the membrane, which is generally identical for most of the aggregates. The edge-to-edge distance of a LH2 complex along the plane of the membrane is 7 nm and the interspace distance between two neighboring LH2 complexes is reasonably small and negligible due to the tight packing of LH2 complexes in an aggregates.

We have carefully confirmed that the linear aggregation feature of LH2 in the membrane is not due to the sample preparations and AFM imaging artifacts, but the intrinsic spatial arrangement within the membranes. This attribution is based on the following evidence: (1) the lower density (LD) membrane samples obtained from the strong light preparation show significantly diluted protein distribution density in the membranes; however, the LH2 proteins in the LD membranes still show linear aggregation, although more spatial separation among the linear aggregates is observed.[32] The evidence that both high density (HD) and LD membranes show similar linear aggregation suggests that the aggregation is not due to spatial congestion of the individual LH2 proteins in the membranes. (2) The random orientations of the linear aggregates (Fig. 3A) indicate that the aggregation is not due to rinsing of the sample by the buffer solution. (3) Our previous and present observation of spectroscopic red shift in adsorption and emission and shorter lifetime components indicate the presence of coupling between LH2 molecules. Based on the evidence, we conclude that the linear aggregation is an intrinsic property of the LH2 proteins in the membranes, at least for the studied species, and the aggregation due to the protein–protein interaction is important for an efficient energy transfer process in the photosynthetic membranes.

We have conducted spectroscopic studies of LH2 complexes to identify the existence of aggregated LH2 in the photosynthetic membrane (Fig. 4) by obtaining and analyzing the absorption and the fluorescence spectra of purified LH2 and membrane fragments of wild-type *Rhodobacter sphaeroides*

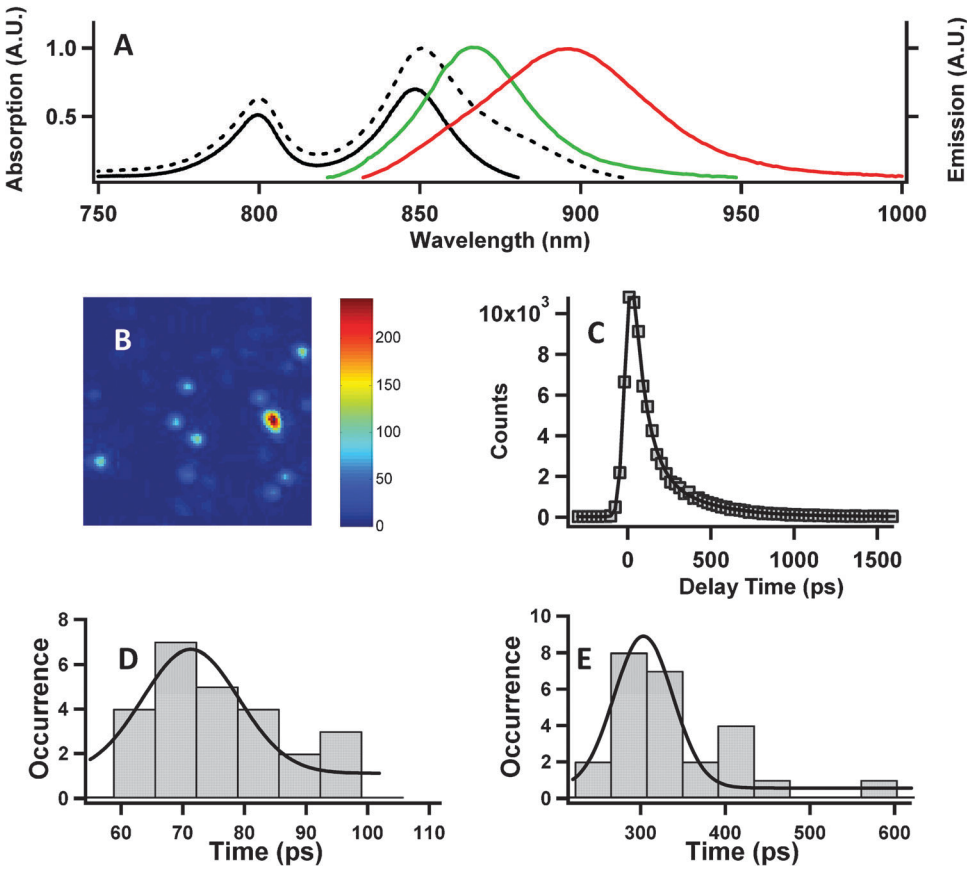

Fig. 4 Steady-state spectroscopic analysis of the membrane LH2 complexes. (A) Absorption of the purified LH2 (black solid line), absorption of the membrane LH2 (black dashed line), fluorescence spectra of purified LH2 (green line) and fluorescence spectra of membrane LH2 (red line). (B) Fluorescence image (15 μm × 15 μm) of the membrane LH2. Each bright spot represents a single membrane fragment with aggregated and/or non-aggregated LH2 complexes. (C) Fluorescence lifetime trace measured from a single membrane fragment (grey squares) and the bi-exponential fitting of the decay (black line). (D) Distribution of the fast component of the lifetime and (E) distribution of the slow component of the lifetime. Gaussian fittings of the distributions are shown with the black solid line.

(strain 2.4.1). The wavelength at the maximum of the absorption profile of purified LH2 is 848 nm. Whereas, in the membrane LH2, the maximum is 2.0 ± 0.2 nm red shifted than that of the purified LH2 (Fig. 4A). The fluorescence maximum of membrane LH2 peaks at 895 nm, about 30 nm red shift from the fluorescence maximum of purified LH2 (866 nm) (Fig. 4A). The fluorescence spectrum of the membrane LH2 shows a small shoulder at 866 nm indicating the presence of non-aggregated LH2 complexes in the membrane in addition to the aggregated complexes. The 30 nm red shift of the emission maximum implies that the energetic coupling of the LH2 complexes in the photosynthetic membrane, which lowers the transition energy by delocalizing the electronic interaction among the whole aggregated structure, is a typical consequence of aggregation associated energetic interaction.

The fluorescence lifetimes measured from the membrane fragments also suggest the existence of energetically coupled aggregated LH2 complexes in the photosynthetic membranes. Fluorescence confocal images (Fig. 4B) are recorded in order to measure the lifetime of single fragments of photosynthetic membranes. The lifetime is measured on each bright spot and each spot represents a single membrane nanoscale fragment. The recorded lifetime decay curves (Fig. 4C) show bi-exponential decays for all of the recorded membrane fragments, which suggest the presence of at least two different structures of LH2 complexes in the photosynthetic membrane. The histograms of magnitudes of the fast and slow components of the bi-exponential decays are shown in Fig. 4D and E4. The Gaussian fitting of each histogram gives the maxima at 71 ± 2 ps and 303 ± 5 ps for the fast and slow decay components, respectively. The slow component is in the same time scale with the lifetimes of the purified LH2 complexes and the reported values,[62,63] and the fast component can be attributed to the aggregated LH2 in the membrane.

We have calculated the absorption, emission and lifetime of each aggregated state of the LH2 complexes by using our aggregation energetic coupling model analysis discussed in the above calculation section. The experimentally recorded absorption and emission wavelengths of the purified LH2 complexes are assumed to be similar to the non-aggregated LH2 complexes in the membrane. The energy of the transition is calculated using eqn (2). After calculating the coupling constant (J_{ij}) of each aggregated state from eqn (1), the energy of the transition for each aggregated state is calculated using eqn (3) and is converted to wavelength from eqn (2). The following

Table 1 The calculated absorption, emission wavelengths and lifetimes for LH2 complexes

Number of LH2 complexes in an aggregate	Absorption wavelength (nm)	Emission wavelength (nm)	Lifetime (ps)
1	848	866	288.3
2	849.09	873.09	144.2
3	850.31	881.21	96.10
4	851.58	889.75	72.07
5	852.87	898.58	57.66
6	854.17	907.65	48.05
7	855.48	916.93	41.19
8	856.80	926.44	36.03

equation is derived from eqn (4) to calculate the fluorescence lifetime of the non-aggregated LH2 complexes in the membrane.

$$\tau = \frac{3h^4\varepsilon_0 c^3 \phi}{16\pi^3 (\Delta E^{ex})^3 \mu^2 \hat{n}} \quad (11)$$

Then the calculated lifetime is used in eqn (6) in order to calculate the lifetimes of aggregated structures. The transition dipole moment for emission is determined from eqn (10) before calculating the emission transition energies for the aggregated LH2 complexes.

All the calculated values of the absorption and emission wavelengths and lifetime for the aggregated LH2 complexes in the photosynthetic membrane are summarized in the Table 1, and the relationship of these data sets are presented in Fig. 5.

The calculated result of the fluorescence lifetime using aggregate energetic coupling theory[35] supports the attribution of the existence of the aggregated LH2 complexes in the photosynthetic membrane. The calculated non-aggregated LH2 lifetime is 288.30 ps (Table 1) which is close to the experimentally determined value of the slow decay component, 303 ± 5 ps. Since the AFM images show the tetramers and the pentamers as the highest populated aggregates in the membrane (Fig. 3B), the aggregate energetic coupling model predicts that the fast component of the lifetime decays is about 72.07–57.66 ps. Supporting this prediction, the experimentally measured lifetime for the fast component is 71 ± 2 ps indicating that the model of the aggregation of LH2 complexes is close to the native structural arrangement of the LH2 complexes in the photosynthetic membrane.

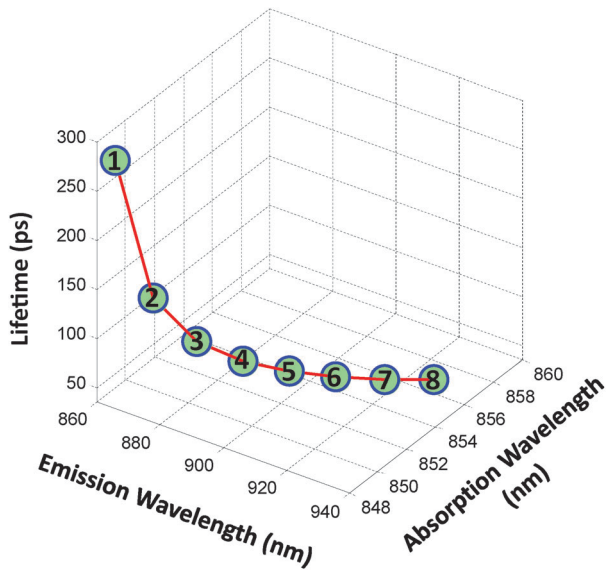

Fig. 5 The relationship of the calculated values of the absorption, emission and lifetime of the LH2 aggregates. The experimentally measured absorption and emission wavelengths of purified LH2 are used for non-aggregated LH2 complexes (monomers). The number in the circle indicates the number of LH2 complexes in the aggregate.

We have also calculated the absorption and emission spectral maxima of the aggregated LH2 complexes using the aggregate theoretical model. The experimentally observed absorption (848 nm) and emission (866 nm) maximum values of the purified (non-aggregated) LH2 are used as the starting parameters to calculate the absorption and the emission peak wavelengths of the aggregated LH2 complexes. The experimental absorption maximum of the membrane LH2 is 850 nm while the calculated absorptions for the aggregated LH2 complexes are ranging from 849.09 nm to 856.80 nm (dimer to octamer). The population distribution of the aggregated LH2 complexes in the membrane suggests that the maximum absorption of the photosynthetic membrane appears around the tetramer and pentamer absorptions since they have the highest occurrence in the photosynthetic membrane.

In calculating the absorption spectrum of the membrane LH2 by using the aggregate theoretical model, we only focus on fitting the 850 nm absorption band, omitting the analysis of the 800 nm absorption band. The absorption band with the highest intensity in the near infrared region maximizes at 848 nm for purified LH2 and can be fitted with Gaussian function (Fig. 6A). We have assumed that the shape and the full width of half maximum (FWHM) of this band in the aggregated LH2 complexes remained the same as those of the absorption band of the purified (non-aggregated) LH2 complexes. The fitted Gaussian curve of the purified LH2 absorption (Fig. 6A) is shifted to each calculated absorption peak value (Table 1) as the maximum of the fitted curve to be the calculated peak value. Then the population weight factor of each aggregated LH2 is included to generate the absorption spectrum of each aggregated LH2 complex (Fig. 6B). These calculated spectral bands are combined to generate the calculated absorption band for the membrane LH2 with the contribution of all the non-aggregated and aggregated LH2 absorptions.

The calculated and experimentally recorded absorption spectra of membrane LH2 complexes are shown in Fig. 6C. A zoom-in view of the peak region of the calculated and experimental absorption spectra is shown in the inset of Fig. 6C. The calculated spectrum closely agrees with the experimental absorption spectrum of membrane LH2 complexes (Fig. 6C). The maximum wavelength of the experimental absorption of membrane LH2 is at 850 nm while the maximum of the calculated absorption is at 850.85 nm. The calculated and experimental values are consistent with our AFM topographic imaging results, which supports our attribution of the existence of the energetically coupled linear aggregate LH2 complexes in

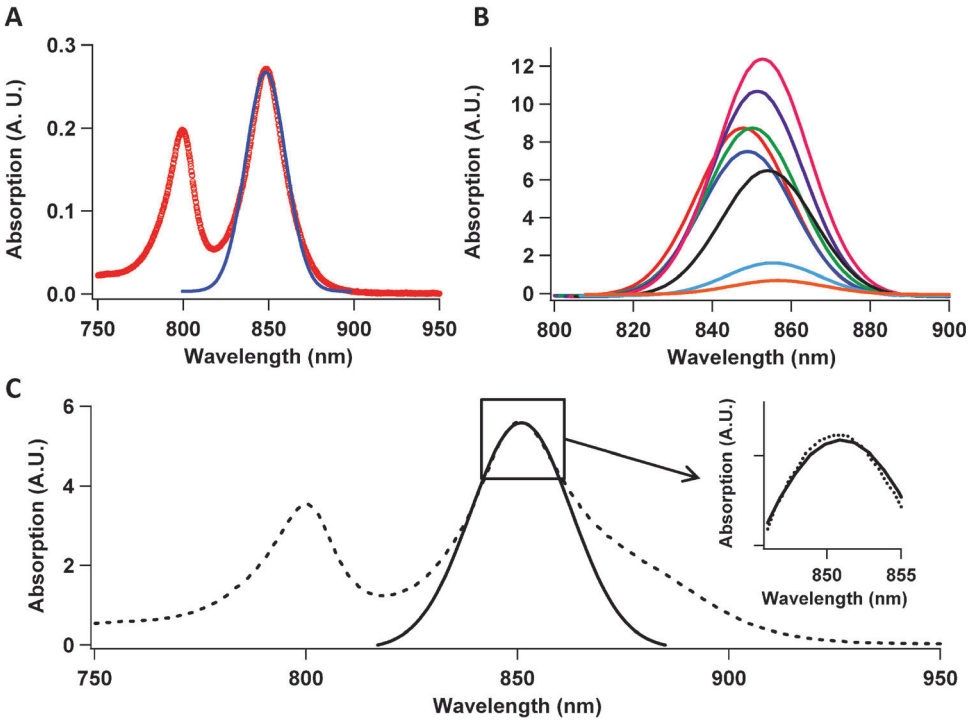

Fig. 6 Calculated and experimental absorption spectra. (A) The absorption spectrum of purified LH2 (red circle) and the Gaussian fit (blue line) for the 848 nm band. (B) Absorption of each LH2 aggregate with the contribution of the population in the membrane (red-monomer, blue-dimer, green-trimer, purple-tetramer, pink-pentamer, black-hexamer, cyan-heptamer and orange-octamer). (C) Calculated absorption spectrum (solid black line) and experimental absorption spectrum of (dashed black line) membrane LH2. The inset shows a zoom-in view of the peak region.

the photosynthesis membrane. The shape and the FWHM of the calculated spectrum essentially fit the experimental absorption spectrum except for the shoulder at 875 nm typically arising from the absorption of LH1 complexes. Nevertheless, we note that our theoretical model results do not necessarily fit the broad line shape of the 850 nm band (Fig. 6C) as we did not include the contribution of the inhomogeneous broadening of the absorption spectra and the possible existence of the longer *J* aggregated LH2 complexes with 8 or more LH2 proteins.

Furthermore, we have analyzed the emission peak positions of the aggregated LH2 complexes using the theoretical aggregate model. The transition dipole moment of the emission of the LH2 complexes is calculated to be 63.45 D using eqn (10), approximately 2.5 times higher than the excitation transition dipole moment. The calculated emission wavelengths of the aggregated LH2 complexes are listed in Table 1. The emission wavelength of the octamer has a red shift at about 60 nm from the emission wavelength of purified LH2 of 866 nm. The population distribution histogram of the aggregated and non-aggregated LH2 complexes in the photosynthetic membrane (Fig. 3B) indicates the maximum of emission to be positioned close to the tetramer and pentamer emissions, at 889.75 nm and 898.75 nm. Similar to the calculation of the absorption spectrum of membrane LH2, we have assumed that the shape and the FWHM of the aggregated LH2 emission spectra remain the same as those of the purified LH2. The emission of purified LH2 complexes is fitted with Asymmetric Double Sigmoidal (ADS) function[64–66] and the experimental emission spectrum of purified LH2 complexes (red circle) and ADS fit (blue line) are shown in Fig. 7A. Fig. 7B shows the emission spectra of non-aggregated LH2 complexes and the aggregated LH2 complexes with the contribution of population of each component in the native photosynthetic membrane. The peak positions of the spectra are identified according to the maxima of the emission peak wavelengths calculated using aggregate theory (Table 1). All the spectra in Fig. 7B are added to generate the emission spectrum of membrane LH2 complexes. Fig. 7C presents the calculated emission spectrum of membrane LH2 as a solid black line and the experimental emission spectrum as a dashed black line. The calculated spectrum peaks at 891 nm, a 4 nm deviation ($\Delta\lambda$ in Fig. 7C) from the experimentally recorded emission spectrum of the membrane LH2 complexes which gives the maximum at 895 nm. The calculated spectrum maintains the shape approximately similar to that of the experimentally recorded spectrum and the difference in FWHM of the two emission spectra is <1.5 nm. The experimentally measured FWHM of the membrane LH2 complexes is 63.01 nm and for the calculated spectrum, the FWHM is 61.60 nm. These values of the calculated and experimental emission spectra of membrane LH2 complexes support our observation of the linearly aggregated LH2 complexes in the membrane.

Generally, solvents, detergents, lipid components, local molecular interactions can perturb LH2 spectroscopy properties. For example, multi-exponential lifetime decays, red-shifted absorption, and red-shifted emission for LH2 in the membrane compared to those for LH2 in the detergent have been reported previously.

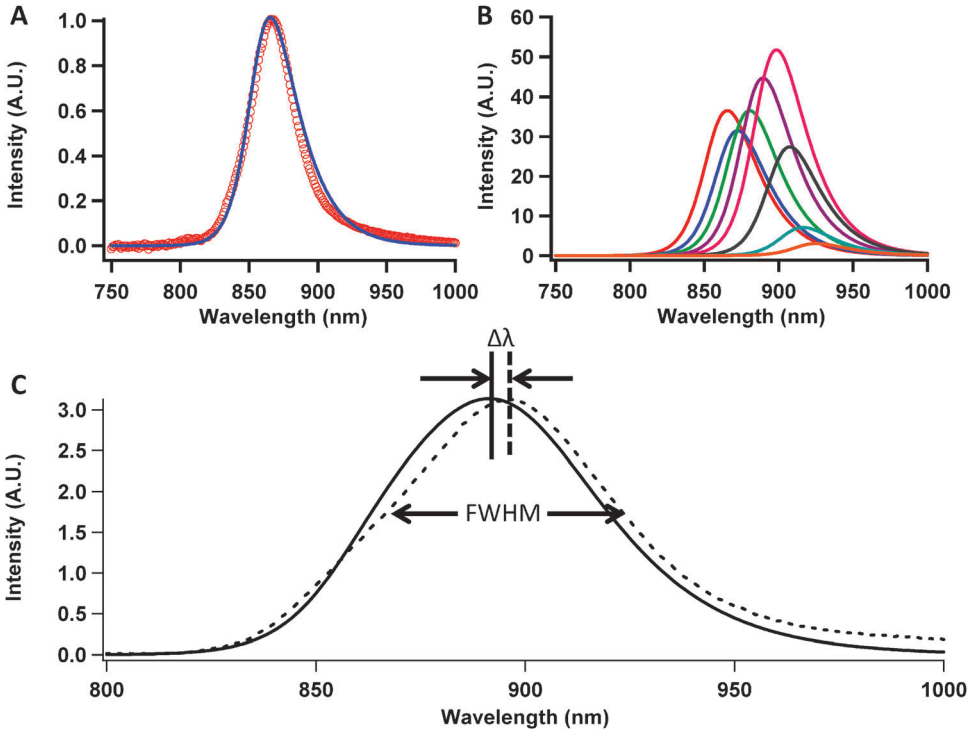

Fig. 7 Calculated and experimental fluorescence spectra. (A) Emission spectrum of purified LH2 (red circle) and asymmetric double sigmoidal fit (blue line). (B) Emission of each LH2 aggregate with the contribution of the population (red-monomer, blue-dimer, green-trimer, purple-tetramer, pink-pentamer, black-hexamer, cyan-heptamer and orange-octamer). (C) The calculated emission spectrum of LH2 according to the population distribution of LH2 complexes in the membrane (solid black line) and the experimental emission spectrum of membrane LH2 (dashed black line).

Intriguingly, this shifting was proved to be due to clustering of the LH2 complexes in the membrane but not due to the interference of detergents.[67,68] This result is consistent with our result that there is a 2 nm spectral red shift between LH2 in the membrane and purified LH2 in buffer with detergents. Nevertheless, our results, by a combined spectroscopic and AFM topographic imaging, for the first time demonstrate the detailed configuration and distribution of the LH2 aggregation from a monomer to a multimer of up to 8 LH2 molecules within an aggregate. The detailed configuration topographic results provide the linear configuration of the aggregates and the titled angles of the monomer LH2 within an aggregate. Based on the topographic configuration, geometry, and the distribution of aggregates in native photosynthetic membranes, we have used the aggregate model analysis based on the exciton coupling modeling to calculate the population-weight averaged absorption, emission, and fluorescence lifetime decays, demonstrating a good fit to our experimental spectroscopic results. Overall, we were able to show that the small $\sim$2 nm red-shift absorption and large $\sim$30 nm red-shift emission are due to a distribution-averaged spectroscopic response that originated from linear aggregate formation in various degrees in the membranes. The close agreement between the experimental and calculated values implies the validity of our attribution of the linear LH2 aggregates in the native photosynthetic membranes.

We note that the model itself has limitations due to its dependence on assumptions to calculate the experimentally observed parameters. The major assumptions we used are: (1) the direction of the transition dipole moment of the emission; and (2) the shape and the FWHM of the calculated spectra for both absorption and emission. We consider that the angle of the transition dipole moment of emission is the same as that of the transition dipole moment of absorption, however, the exact angle is yet to be identified. An experimentally determined angle for the transition dipole moment of emission, although beyond the scope of this work, will further enhance the accuracy of the calculation. Furthermore, we consider that the shape and FWHM do not change in aggregated LH2 complexes since the number of LH2 complexes in an aggregate is significantly small to generate a major deviation. Although the membrane fragments with only one type of aggregated LH2 complex (all the aggregates with the same number of LH2 complexes) are currently impossible to produce, such membrane fragments will help to determine the exact position of the absorption and emission spectra of aggregated LH2 complexes. Also, the thermal broadening of the spectra of membrane fragments makes it difficult to separate and analyze the individual contribution of each aggregated state of the membrane LH2 complexes under physiologically relevant conditions while such separation can be expected at low temperature analysis. Therefore, further experimental approaches are needed to characterize the aggregation of membrane LH2 complexes. In addition to the abovementioned approaches, using tip-enhanced AFM or near-field spectroscopic imaging analysis for individual aggregates simultaneously by

topographic and spectroscopic nanoscale analysis will be highly informative and powerful, which is ongoing in our laboratory.

Recently, a number of reported studies on similar light harvesting photosynthetic systems observed similar red-shifted emission spectra and provided insightful model analyses.[70–94] For example, the red-shifted emission spectra observed for the photosystem I of *T. elongates* and *A. platensis* were attributed to the formation of the trimer out of the monomer photosystem I proteins.[69–71] Also, an exciton self-trapping model[72–87] associated with electron–phonon coupling has been developed and suggested to understand the red-shift emission spectra of the single-molecule LH2 proteins[72–74,88–92] as well as the ensemble-averaged emission spectra of the photosynthetic membrane at low temperature.[73,74,76,82] Nevertheless, it is likely that the self-trapping effect can be significantly weakened at room temperature and in solution. Furthermore, the LH2 aggregation related emission spectral changes and fluorescence lifetime changes have also been systematically studied in aqueous solutions.[93]

The biological implication and relevance of the LH2 linear aggregation in photosynthetic membranes at room temperature are significant for light harvesting functions. Besides that the linear aggregates of LH2 facilitate efficient long distance energy transfer, the finite aggregate length architecture of the LH2 linear aggregates ensures the redundancy of avoiding that LH2 energetic coupling defects sink the energy transfer in the photosynthetic membranes. Recently, a membrane texture analysis suggested that the texture of photosynthetic membrane patches changes from rigid to flexible when the LH2 proteins are removed from the membrane by mutation,[94] which is consistent with the existence of the linear aggregates of LH2 that enhance the mechanic strength of the membranes. Nevertheless, our works, this work on model analysis of the LH2 energy coupling in aggregates, and our previous work on spectroscopic and topographic analyses of LH2 linear aggregation[32] so far only provide a partial understanding of the complex light harvesting protein systems, and further characterization and comprehension of the energy transfer and coupling mechanisms and dynamics are definitely needed. Ultimately, the perspective that the LH2 aggregate may significantly impact the light harvesting efficiency in the photosynthetic membrane relies on the direct measurements of the LH2–LH1 energy transfer, which is beyond the scope of this work. Although we have observed in our AFM imaging analysis that the LH1 can be closely localized with the LH2 aggregates, we have not focused on studying the energy transfer between the LH2 and LH1 proteins because the primary samples we used are LH1 knocked out membranes for our specific focus on studying intermolecular energy transfer among the LH2 proteins. A more complete molecular-level understanding will most likely arise from a combined analysis involving spectroscopic, topographic, and theoretical modeling characterizations of the photosynthetic membranes at both ensemble-averaged and single-molecule levels in both temporal and frequency domains at room temperature. Our work reported here on LH2 aggregate energy coupling model analysis based on the AFM imaging and spectroscopic characterization provides a step forward in the investigation of the intermolecular LH2 spectral dynamics and mechanism by using such combined experimental and theoretical approaches.

Conclusion

We have characterized the existence of the inhomogeneous linear aggregated LH2 complexes in the photosynthetic membrane of purple bacteria by using AFM, spectroscopy analysis and aggregate energetic coupling theoretical calculations. The tilted angle of the LH2 monomers in the aggregated complexes to the plane of the membrane and the population distribution of LH2 aggregates in the photosynthetic membranes are determined from the AFM image analysis. The maxima of the absorption and emission of non-aggregated LH2 complexes are determined by using the purified LH2 complexes. We have developed and used the aggregate model analysis to calculate the lifetimes, absorption and emission wavelengths of each aggregated state of LH2 complexes. The calculated absorption spectrum of the native membrane LH2 in the presence of all the non-aggregated and aggregated LH2 complexes agrees with the experimentally recorded absorption spectrum (<1 nm), and the calculated emission spectral maximum of the membrane LH2 is close to the experimental emission wavelength by 4 nm. Not only the maximum of the calculated emission wavelength is in the same scale as the experimentally observed emission wavelength, but also the shape and the FWHM of the emission spectrum show an agreement, proving the contribution of all the non-aggregated (monomer) and aggregated (dimer to octamer) states of membrane LH2 complexes to the emission spectrum. Furthermore, the close agreement between the experimental and calculated values of the lifetimes, absorption and emission wavelengths confirms the co-existence of non-aggregated and linearly aggregated LH2 complexes in the photosynthetic membrane. We conclude that the major contribution to the fast component of the lifetime comes from the highly populated aggregates in the membrane. The critical and overarching picture is that the configuration and the distribution of the LH2 molecules are highly inhomogeneous rather than homogeneous in a native photosynthetic membrane, so that any in-depth exploration of the physical nature of the averaged spectroscopic characteristics has to come from an analysis involving the characteristics of the spatial and configuration distribution inhomogeneity. Our work provides a novel approach and a consistent aggregation model for analyzing such complex biological systems. The revealing of the existence of the energetically coupled aggregates of LH2 in photosynthetic membranes provides a fundamental knowledge of the light harvesting mechanism in Nature, specifically, of a long distance and high efficient intermolecular energy transfer process in light harvesting processes in photosynthetic membranes.

Acknowledgements

We thank Prof. Samuel Kapalan and Dr Xiaohua Zeng of the Department of Microbiology and Molecular Genetics, the University of Texas Health Science Center, Medical School, 6431 Fannin, Houston, TX 77030, for providing us the

photosynthetic membrane samples. We acknowledge the support of our research from the Office of Basic Energy Sciences Chemical Sciences, Geosciences & Biosciences Division within the Office of Science of the U.S. Department of Energy and the Ohio Eminent Scholar Endowment.

References

1 C. Jungas, J. Ranck, J. Rigaud, P. Joliot and A. Vermeglio, *EMBO J.*, 1999, **18**, 534–542.
2 D. E. Chandler, J. Hsin, C. B. Harrison, J. Gumbart and K. Schulten, *Biophys. J.*, 2008, **95**, 2822–2836.
3 R. J. Cogdell, A. Gall and J. Kohler, *Q. Rev. Biophys.*, 2006, **39**, 227–324.
4 D. Rutkauskas, V. Novoderezhkin, R. J. Cogdell and R. V. Grondelle, *Biophys. J.*, 2005, **88**, 422–435.
5 S. Bahatyrova, R. N. Frese, C. A. Siebert, J. D. Olsen, K. O. van der Werf, R. van Grondelle, R. A. Niederman, P. A. Bullough, C. Otto and C. N. Hunter, *Nature*, 2004, **430**, 1058–1062.
6 G. McDermott, S. M. Prince, A. Freer, A. M. Hawthornthwaitelawless, M. Z. Papiz, R. J. Cogdell and N. W. Isaacs, *Nature*, 1995, **374**, 517–521.
7 T. Walz, S. J. Jamieson, C. M. Bower, P. A. Bullough and C. N. Hunter, *J. Mol. Biol.*, 1998, **282**, 833–845.
8 W. J. Vredenberg and L. N. M. Duysens, *Nature*, 1963, **197**, 355–357.
9 X. Hu, T. Ritz, A. Damjanovic, F. Autenrieth and K. Schulten, *Q. Rev. Biophys.*, 2002, **35**, 1–62.
10 T. Ritz, A. Damjanovic and K. Schulten, *ChemPhysChem*, 2002, **3**, 243–248.
11 M. Z. Papiz, S. M. Prince, T. D. Howard, R. J. Cogdell and N. W. Isaacs, *J. Mol. Biol.*, 2003, **326**, 1523–1538.
12 V. Novoderezhkin, D. Rutkauskas and R. V. Grondelle, *Biophys. J.*, 2006, **90**, 2890–2902.
13 A. W. Roszak, T. D. Howard, J. Southall, A. T. Gardiner, C. J. Law, N. W. Isaacs and R. J. Cogdell, *Science*, 2003, **302**, 1969–1972.
14 J. Deisenhofer, O. Epp, K. Miki, R. Huber and H. Michel, *Nature*, 1985, **318**, 618–624.
15 J. P. Allen, G. Freher, T. O. Yeates, H. Komiya and D. C. Rees, *Proc. Natl. Acad. Sci. U. S. A.*, 1987, **84**, 6162–6166.
16 S. Bahatyrova, R. N. Frese, K. O. van der Werf, C. Otto, C. N. Hunter and J. D. Olsen, *J. Biol. Chem.*, 2004, **279**, 21327–21333.
17 D. Rutkauskas, R. J. Cogdell and R. van Grondelle, *Biochemistry*, 2006, **45**, 1082–1086.
18 V. Sundstrom, T. Pullerits and R. van Grondelle, *J. Phys. Chem. B*, 1999, **103**, 2327–2346.
19 H. van Amerongen, L. Valkunas and R. van Grondelle, *Photosynthetic Excitons*, World Scientific Publishing Co., Singapore, 2000.
20 X. C. Hu, T. Ritz, A. Damjanovic, F. Autenrieth and K. Schulten, *Q. Rev. Biophys.*, 2002, **35**, 1–62.
21 P. Horton, A. V. Ruban, D. Rees, A. A. Pascal, G. Noctor and A. J. Young, *FEBS Lett.*, 1991, **292**, 1–4.
22 M. Z. Papiz, S. M. Prince, A. M. Hawthornthwaitelawless, G. McDermott, A. Freer and N. W. Isaacs, *Trends Plant Sci.*, 1996, **1**, 198–206.
23 R. N. Frese, J. D. Olsen, R. Branvall, W. H. J. Westerhuis, C. N. Hunter and R. van Grondelle, *Proc. Natl. Acad. Sci. U. S. A.*, 2000, **97**, 5197–5202.
24 C. J. Law, R. J. Cogdell and H. W. Trissl, *Photosynth. Res.*, 1997, **52**, 157–165.
25 T. Ritz, S. Park and K. Schulten, *J. Phys. Chem. B*, 2001, **105**, 8259–8267.
26 S. Scheuring, J. Rigaud and J. Sturgis, *EMBO J.*, 2004, **23**, 4127–4133.
27 L. Liu, K. Duquesne, F. Oesterhelt, J. Sturgis and S. Scheuring, *Proc. Natl. Acad. Sci. U. S. A.*, 2011, **108**, 9455–9459.
28 L. Liu, J. Sturgis and S. Scheuring, *J. Struct. Biol.*, 2011, **173**, 138–145.
29 S. Scheuring, J. Sturgis, V. Prima, A. Bernadac, D. Levy and J. Rigaud, *Proc. Natl. Acad. Sci. U. S. A.*, 2004, **101**, 11293–11297.
30 S. Scheuring and J. Sturgis, *Science*, 2005, **309**, 484–487.
31 L. Liu, T. J. Aartsma and R. N. Frese, *FEBS J.*, 2008, **275**, 3157–3166.
32 Y. He, X. Zeng, S. Mukherjee, S. Rajapaksha, S. Kaplan and H. P. Lu, *Langmuir*, 2010, **26**, 307–313.
33 D. Pan, D. Hu, R. Liu, X. Zeng, S. Kaplan and H. P. Lu, *J. Phys. Chem. C*, 2007, **111**, 8948–8956.
34 W. Humphrey, A. Dalke and K. Schulten, *J. Mol. Graphics*, 1996, **14**, 33–38.
35 T. Kobayashi, *J aggregates*, World Scientific Publishing Co., Singapore, 1996.
36 E. E. Jelley, *Nature*, 1936, **138**, 1009–1010.
37 A. Eisfeld and J. S. Briggs, *Chem. Phys.*, 2006, **324**, 376–384.
38 G. Scheibe, *Angew. Chem.*, 1936, **49**, 563–563.
39 G. Scheibe, *Angew. Chem.*, 1937, **50**, 212–219.
40 S. De Boer and D. A. Wiersma, *Chem. Phys. Lett.*, 1990, **165**, 45–53.
41 A. Tilgner, H. P. Trommsdorff, J. M. Zeigler and R. M. Hochstrasser, *J. Chem. Phys.*, 1992, **96**, 781–796.
42 S. De Boer, K. J. Vink and D. A. Wiersma, *Chem. Phys. Lett.*, 1987, **137**, 99–106.
43 H. Fidder, J. Knoester and D. A. Wiersma, *J. Chem. Phys.*, 1993, **98**, 6564–6566.
44 C. Didraga, V. A. Malyshev and J. Knoester, *J. Phys. Chem. B*, 2006, **110**, 18818–18827.
45 C. Didraga, A. Pugzlys, P. R. Hania, H. Berlepsch, K. Duppen and J. Knoester, *J. Phys. Chem. B*, 2004, **108**, 14976–14985.
46 V. V. Egorov and M. V. Alfimov, *Phys.–Usp.*, 2007, **50**, 985–1029.
47 N. Kato, K. Yuasa, T. Araki, I. Hirosawa, M. Sato, N. Ikeda, K. Iimura and Y. Uesu, *Phys. Rev. Lett.*, 2005, **94**, 136404.
48 H. Sumi, *J. Phys. Chem. B*, 1999, **103**, 252–260.
49 K. Mukai, S. Abe and H. Sumi, *J. Phys. Chem. B*, 1999, **103**, 6096–6102.
50 S. Jang, M. D. Newton and R. J. Silbey, *Phys. Rev. Lett.*, 2004, **92**, 218301.

51 M. Sener, J. Strmpfer, J. Hsin, D. Chandler, S. Scheuring, C. N. Hunter and K. Schulten, *ChemPhysChem*, 2011, **12**, 518–531.
52 K. Sauer, R. J. Cogdell, S. M. Prince, A. Freer, N. W. Isaacs and H. Scheer, *Photochem. Photobiol.*, 1996, **64**, 564–576.
53 S. Scheuring, J. Seguin, S. Marco, D. Levy, C. Breyton, B. Robert and J. Rigaud, *J. Mol. Biol.*, 2003, **325**, 569–580.
54 M. K. Gilson and B. H. Honig, *Biopolymers*, 1986, **25**, 2097–2119.
55 D. C. Mauzerall and C. M. Drain, *Biophys. J.*, 1992, **63**, 1544–1555.
56 J. N. Israelachvili, *Langmuir*, 1994, **10**, 3369–3370.
57 E. E. Ross, L. J. Rozanski, T. Spratt, S. Liu, D. F. O'Brien and S. S. Saavedra, *Langmuir*, 2003, **19**, 1752–1765.
58 R. Monshouwer, M. Abrshamsson, F. van Mourik and R. van Grondelle, *J. Phys. Chem. B*, 1997, **101**, 7241–7248.
59 W. P. F. Ruijter, J. M. Segura, R. J. Cogdell, A. T. Gardiner, S. Oellerich and T. J. Aartsma, *Chem. Phys.*, 2007, **341**, 320–325.
60 A. Kitai, *Luminescent Materials and Applications*, John Wiley & Sons Ltd., West Sussex, 2008.
61 G. S. Smith, *Eur. J. Phys.*, 2010, **31**, 819–825.
62 P. J. Walla, J. Yom, B. P. Krueger and G. R. Fleming, *J. Phys. Chem. B*, 2000, **104**, 4799–4806.
63 V. Barzda, C. J. de Grauw, J. Vroom, F. J. Kleima, R. van Grondelle, H. van Amerongen and H. C. Gerritsen, *Biophys. J.*, 2001, **81**, 538–546.
64 D. Marinov, J. M. Rey, M. G. Muller and M. W. Sigrist, *Appl. Opt.*, 2007, **46**, 3981–3986.
65 J. Krustok, H. Collan, M. Yakushev and K. Hjelt, *Phys. Scr.*, 1999, **T79**, 179–182.
66 V. Moshnyaga, K. Gehrke, O. I. Lebedev, L. Sudheendra, A. Belenchuk, S. Raabe, O. Shapoval, J. Verbeeck, G. Van Tendeloo and K. Samwer, *Phys. Rev. B: Condens. Matter Mater. Phys.*, 2009, **79**, 134413.
67 T. Pflock, M. Dezi, G. Venturoli, R. J. Cogdell, J. Kohler and S. Oellerich, *Photosynth. Res.*, 2008, **95**, 291–298.
68 M. F. Richter, J. Baier, R. J. Cogdell, J. Kohler and S. Oellerich, *Biophys. J.*, 2007, **93**, 183–191.
69 M. Hussels and M. Brecht, *Biochemistry*, 2011, **50**, 3628–3637.
70 M. Hussels, J. B. Nieder, C. Elsaesser and M. Brecht, *Acta Phys. Pol., A*, 2012, **122**, 269–274.
71 M. Hussels and M. Brecht, *FEBS Lett.*, 2011, **585**, 2445–2449.
72 R. Kunz, K. Timpmann, J. Southall, R. J. Cogdell, A. Freiberg and J. Koehler, *J. Phys. Chem. B*, 2012, **116**, 11017–11023.
73 A. Freiberg, M. Ratsep, K. Timpmann, G. Trinkunas and N. W. Woodbury, *J. Phys. Chem. B*, 2003, **107**, 11510–11519.
74 K. Timpmann, Z. Katiliene, N. W. Woodbury and A. Freiberg, *J. Phys. Chem. B*, 2001, **105**, 12223–12225.
75 A. Freiberg, K. Timpmann, S. Lin and N. W. Woodbury, *J. Phys. Chem. B*, 1998, **102**, 10974–10982.
76 K. Timpmann, M. Ratsep, C. N. Hunter and A. Freiberg, *J. Phys. Chem. B*, 2004, **108**, 10581–10588.
77 M. Ketelaars, C. Hofmann, J. Kohler, T. D. Howard, R. J. Cogdell, J. Schmidt and T. J. Aartsma, *Biophys. J.*, 2002, **83**, 1701–1715.
78 M. F. Richter, J. Baier, J. Southall, R. J. Cogdell, S. Oellerich and J. Kohler, *Proc. Natl. Acad. Sci. U. S. A.*, 2007, **104**, 20280–20284.
79 T. Pullerits, M. Chachisvilis and V. Sundstrom, *J. Phys. Chem.*, 1996, **100**, 10787–10792.
80 V. Novoderezhkin, R. Monshouwer and R. van Grondelle, *J. Phys. Chem. B*, 1999, **103**, 10540–10548.
81 G. Trinkunas and A. Freiberg, *J. Lumin.*, 2006, **119**, 105–110.
82 A. Freiberg and G. Trinkunas, *Photosynthesis in silico* Understanding Complexity From Molecules to Ecosystems, ed. A. Laisk, L. Nedbal and Govindjee, Springer, Netherlands, 2009, vol. 29, pp. 55–82.
83 H. Sumi and A. Sumi, *J. Phys. Soc. Jpn.*, 1994, **63**, 637–657.
84 Y. Toyozawa, *Optical Processes in Solids*, ed. Y. Toyozawa, Cambridge University Press, Cambridge, 2003.
85 J. Knoester and V. M. Agranovich, *Frenkel and Charge-Transfer Excitons in Organic Solids*, Elsevier, Amsterdam, 2003, vol. 31, pp. 1–96.
86 Y. Toyozawa, *Prog. Theor. Phys.*, 1958, **20**, 53–81.
87 in *Excitions*, ed. E. I. Rashba and M. D. Sturge, North-Holland Publishing Company, Amsterdam, 1982.
88 A. Freiberg, M. Ratsep, K. Timpmann and G. Trinkunas, *J. Lumin.*, 2003, **102**, 363–368.
89 K. Timpmann, A. Ellervee, A. Kuznetsov, A. Laisaar, G. Trinkunas and A. Freiberg, *J. Lumin.*, 2003, **102**, 220–225.
90 K. Timpmann, A. Ellervee, T. Pullerits, R. Ruus, V. Sundstrom and A. Freiberg, *J. Phys. Chem. B*, 2001, **105**, 8436–8444.
91 A. Freiberg, R. Ruus and K. Timpmann, in *Spectroscopy of Biological Molecules: New Directions*, ed. J. Greve, G. J. Puppels and C. Otto, Springer, Netherlands, 1999, pp. 115–118.
92 K. Timpmann, N. W. Woodbury and A. Freiberg, *J. Phys. Chem. B*, 2000, **104**, 9769–9771.
93 F. Yang, L.-J. Yu, P. Wang, X.-C. Ai, Z.-Y. Wang and J.-P. Zhang, *J. Phys. Chem. B*, 2011, **115**, 7906–7913.
94 C. A. Siebert, P. Qian, D. Fotiadis, A. Engel, C. N. Hunter and P. A. Bullough, *EMBO J.*, 2004, **23**, 690–700.